





Article

High-Molecular-Weight PLA-*b*-PEO-*b*-PLA Triblock Copolymer Templated Large Mesoporous Carbons for Supercapacitors and CO₂ Capture

Mohamed Gamal Mohamed ¹, Wei-Shih Hung ¹, Ahmed F. M. EL-Mahdy ¹,
Mahmoud M. M. Ahmed ¹, Lizong Dai ², Tao Chen ³ and Shiao-Wei Kuo ^{1,4,*}

¹ Department of Materials and Optoelectronic Science, Center of Crystal Research, National Sun Yat-Sen University, Kaohsiung 80424, Taiwan; mgamal.eldin12@yahoo.com (M.G.M.); m063100027@student.nsysu.edu.tw (W.-S.H.); ahmed1932005@gmail.com (A.F.M.E.-M.); kuosw19760501@gmail.com (M.M.M.A.)

² Fujian Provincial Key Laboratory of Fire Retardant Materials, College of Materials, Xiamen University, Xiamen 361005, China; lzdai@xmu.edu.cn

³ Ningbo Institute of Material Technology and Engineering, Chinese Academy of Science, Zhongguan West Road 1219, Ningbo 315201, China; tao.chen@nimte.ac.cn

⁴ Department of Medicinal and Applied Chemistry, Kaohsiung Medical University, Kaohsiung 807, Taiwan

* Correspondence: kuosw@faculty.nsysu.edu.tw; Tel.: +886-7-525-4099

Received: 1 May 2020; Accepted: 20 May 2020; Published: 23 May 2020



Abstract: High-molecular-weight PLA₄₄₀-*b*-PEO₄₅₄-*b*-PLA₄₄₀ (LEL) triblock copolymer was synthesized through simple ring-opening polymerization (ROP) by using the commercial homopolymer HO-PEO₄₅₄-OH as the macro-initiator. The material acted as a single template to prepare the large mesoporous carbons by using resol-type phenolic resin as a carbon source. Self-assembled structures of phenolic/LEL blends mediated by hydrogen bonding interaction were determined by FTIR and SAXS analyses. Through thermal curing and carbonization procedures, large mesoporous carbons (>50 nm) with a cylindrical structure and high surface area (>600 m²/g) were obtained because the OH units of phenolics prefer to interact with PEO block rather than PLA block, as determined by FTIR spectroscopy. Furthermore, higher CO₂ capture and good energy storage performance were observed for this large mesoporous carbon, confirming that the proposed approach provides an easy method for the preparation of large mesoporous materials.

Keywords: hydrogen bonding; triblock copolymer; CO₂ capture; supercapacitors and mesoporous carbon

1. Introduction

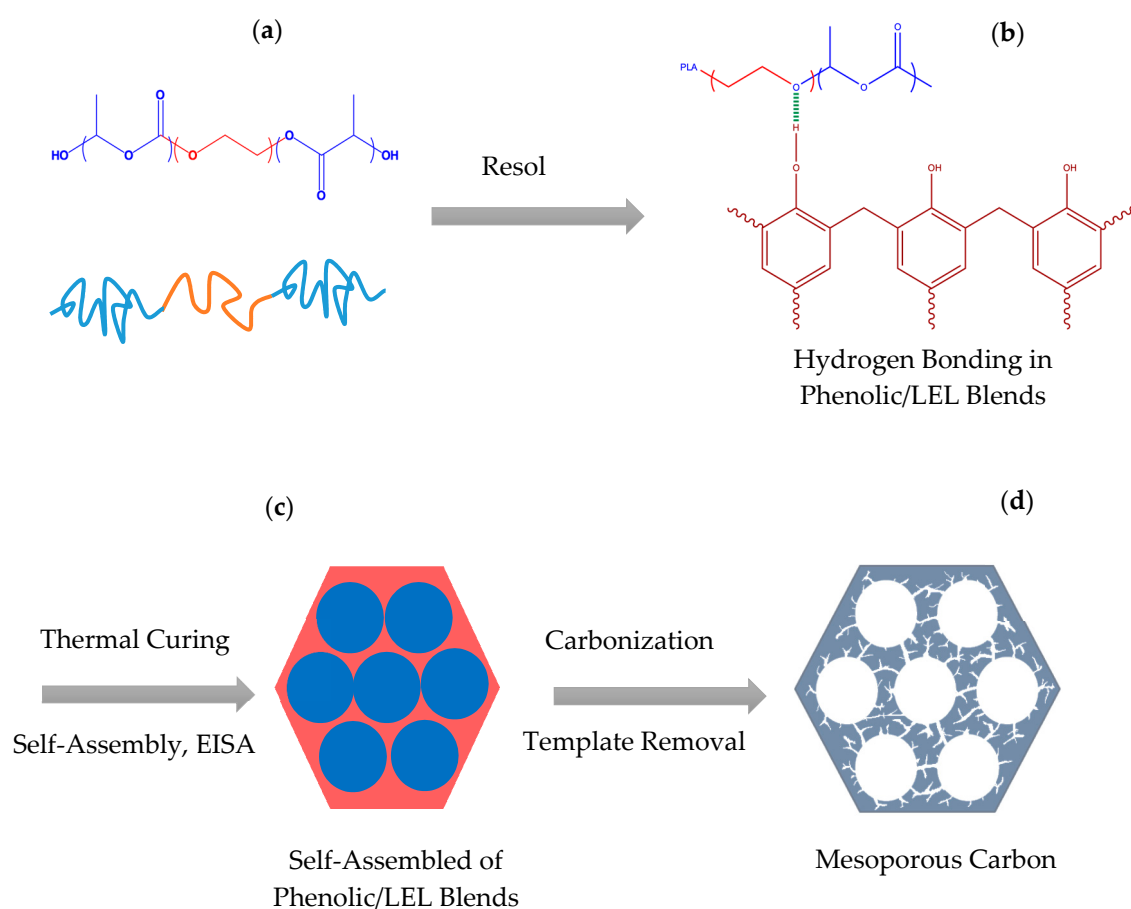
The high surface areas and pore volumes of porous materials are very interesting for different applications, including energy storage, adsorption, drug delivery, and catalysis [1–13]. Based on their pore sizes, three different kinds of porous materials are defined from the IUPAC rules, including microporous (<2 nm), mesoporous (2–50 nm), and macroporous (>50 nm) materials.

In general, the preparation of mesoporous silicas, phenolic resin, or carbons templated by block copolymer is the most common approach compared with foaming, phase separation, hard-template, and molecular imprinting methods [14–17]. Using this approach, well-defined mesoporous structures can be obtained since the block copolymer could be self-assembled into different structures through microphase separation connected by covalent bond [18–20]. The concept of mediating the hydrogen bonding strength in block copolymer mixtures [21–32] to synthesize mesoporous materials has been widely discussed in our previous studies [18,19,33–35]. Using a commercial pluronic-type poly(ethylene oxide-*b*-propylene oxide-*b*-ethylene oxide) triblock copolymer as the template is the most widely used approach to preparing

mesoporous materials; however, because of the limitation presented by the molecular weight of this kind of triblock copolymer, it is difficult to prepare mesoporous phenolic or carbon with pore size >10 nm [36–41]. As a result, using a high-molecular-weight long hydrophobic block in a PEO-based block copolymer including poly(ethylene-oxide-*b*-styrene) (PEO-*b*-PS) [42–44], poly(ethylene oxide-*b*-caprolactone) (PEO-*b*-PCL) [33–35,45–47], poly(ethylene-oxide-*b*-methyl methacrylate) (PEO-*b*-PMMA) [48], or poly(ethylene oxide-*b*-lactic acid) (PEO-*b*-PLA) [49,50] as the templates is the easiest way to prepare large mesoporous materials. For example, employing PEO₁₂₅-*b*-PS₂₃₀ and PEO₁₁₄-*b*-PLA₉₄ diblock copolymers as a template could provide the large pore size (23 and 21 nm, respectively) required to prepare mesoporous carbon [42,50]. In addition, the high molecular weight of PEO-*b*-PS-*b*-PI triblock copolymer (ca. 100 kDa) as a single template was used to obtain a mesoporous carbon with large pore size (39 nm) [51].

Zhao et al. proposed another method to further increase the pore size of mesoporous materials by using PEO-*b*-PMMA/PMMA or PEO-*b*-PS/PS blend as a co-template to obtain large mesoporous materials, in which either the homopolymer PMMA or PS could act as the pore expander. However, macrophase separation may occur at higher homopolymer concentrations (>20 wt.%) that would induce disordered mesoporous materials with multimodal pore sizes (ca. 40–90 nm) [52,53]. Furthermore, the high-molecular-weight PEO-*b*-PMMA and PEO-*b*-PS diblock copolymers are difficult to synthesize from the chain end modification of the PEO block segment (such as PEO-Br) by atom transfer radical polymerization [42,48]. Therefore, the high-molecular-weight triblock copolymer PCL-*b*-PEO-*b*-PCL (ca. 120 kDa) was synthesized through simple ring-opening polymerization (ROP) using simple HO-PEO₄₅₄-OH as the macro-initiator in our previous study [54]. A large number of macroporous carbons with a pore size larger than 50 nm could be obtained using this PCL-*b*-PEO-*b*-PCL triblock copolymer, in which the resol phenolic resin also acts as the carbon source [54]. We also observed that the hydrogen bonding interaction between phenolic resin and those hydrophobic block segments played an important role in the determination of the pore size of mesoporous carbons [50]. For example, the weak hydrogen bonding interaction of PCL (inter-association equilibrium constant (K_A) = 116) [55] and PMMA (K_A = 20) segment [56,57] induced thicker walls but smaller pore size in mesoporous carbons as compared with PS or PLA segments having similar molecular weight. This phenomenon was due to the lack of hydrogen bonding interaction between the phenolic and PS segment. Thus, the PS or PLA segment could undergo complete microphase separation and induce thinner walls, but a larger pore size of mesoporous carbons could only be obtained after the template was removed [50].

In this study, we also synthesized a relatively higher molecular weight PLA₄₄₀-*b*-PEO₄₅₄-*b*-PLA₄₄₀ (LEL) triblock copolymer using HO-PEO₄₅₄-OH as the macro-initiator by simple ROP. Compared with the PEO₁₁₄-*b*-PLA₉₄ diblock copolymer [50], this LEL triblock copolymer possessed high molecular weight as a template and thus could provide large mesoporous carbons as expected. In addition, as also compared with PCL-*b*-PEO-*b*-PCL triblock copolymer, using the PLA-*b*-PEO-*b*-PLA triblock copolymer as the template had two advantages, including: (1) No crystallization of the PLA segment of the template occurred since the self-assembled structure strongly affected the microphase separation from the crystallization of the PCL segment [49]; (2) The very weak hydrogen bonding interaction of the PLA segment could provide larger pore size of mesoporous carbons with a hydrophobic segment having a similar molecular weight [50]. Therefore, a mesoporous carbon with large pore size could be obtained using this LEL triblock copolymer as a template in this study. Scheme 1 shows that the resol-type phenolic resin acted as the carbon source templated by the LEL triblock copolymer through thermal curing and carbonization procedures. First we discuss the hydrogen bonding and self-assembled nanostructures of phenolic/LEL blends, and then the self-assembled porous structure, surface area, pore volume, and pore size of these very large mesoporous carbons were also investigated in detail. Furthermore, the applications of these large mesoporous carbons in energy storage and CO₂ capture were enriched by using this simple ROP approach to synthesize this LEL triblock copolymer as a single template.



Scheme 1. (a) Chemical structure of PLA₄₄₀-*b*-PEO₄₅₄-*b*-PLA₄₄₀ (LEL) triblock copolymer; (b) hydrogen bonding interaction in phenolic/LEL blends; (c) thermal-curing-induced self-assembled structure of phenolic/LEL blends; (d) fabrication of mesoporous carbon after carbonization.

2. Experimental Section

2.1. Materials

The triblock copolymer PLA₄₄₀-*b*-PEO₄₅₄-*b*-PLA₄₄₀ (LEL) was synthesized using dihydroxyl-terminated poly(ethylene oxide) (PEO₄₅₄) as the macroinitiator, D,L-lactic acid (LA) as a monomer, and stannous(II) octoate as a catalyst through ROP. The LA monomer was introduced into the PEO₄₅₄ macroinitiator under N₂ atmosphere and then stirred at 130 °C for 1 day. The LEL triblock copolymer was dissolved in CH₂Cl₂ and then precipitated in n-hexane and dried under vacuum for 2 days [50]. The molecular weight of resol-type phenolic resin was ca. 500 g/mol, which was synthesized through a condensation reaction in NaOH using phenol and formaldehyde [50,54].

2.2. The Preparation of Mesoporous Carbon

We prepared various phenolic/LEL mixtures with different ratios dissolved in THF, where the carbon source and the template were resol phenolic resin and LEL triblock copolymer, respectively. The mixtures were stirred for 3 days at room temperature, and then the THF solvent was slowly evaporated at room temperature for the evaporation-induced self-assembly (EISA) approach. The powder was then placed into the oven at 150 °C for 48 h for the thermal curing of phenolic resin by the reaction-induced microporous separation mechanism, and the corresponding mesoporous carbon was obtained using thermal calcination for template removal from room temperature to 700 °C at 1 °C/min, as displayed in Scheme 1.

3. Results and Discussion

3.1. Characterizations of Phenolic/PLA-*b*-PEO-*b*-PLA Blend

We first used ROP to synthesize the PLA₄₄₀-*b*-PEO₄₅₄-*b*-PLA₄₄₀ triblock copolymer as a template, and its molecular weight was determined using the ¹H NMR spectrum as displayed in Figure 1. The typical CH₂ protons (peak a) for the PEO segment were located at 3.65 ppm, and the methine (CH, peak b) and methyl (CH₃, peak c) protons for the PLA segment appeared at 5.20 and 1.56 ppm, respectively. The molecular weight of this LEL triblock copolymer could be calculated by the peak area ratio of peak a with peak b, and the triblock copolymer polydispersity was 1.15 based on GPC analysis. Scheme 1 displays the preparation of mesoporous carbon templated by LEL triblock copolymer from the phenolic/LEL blends. The corresponding mesophase was gradually formed by the EISA mechanism, further thermal curing, and carbonization for template removal.

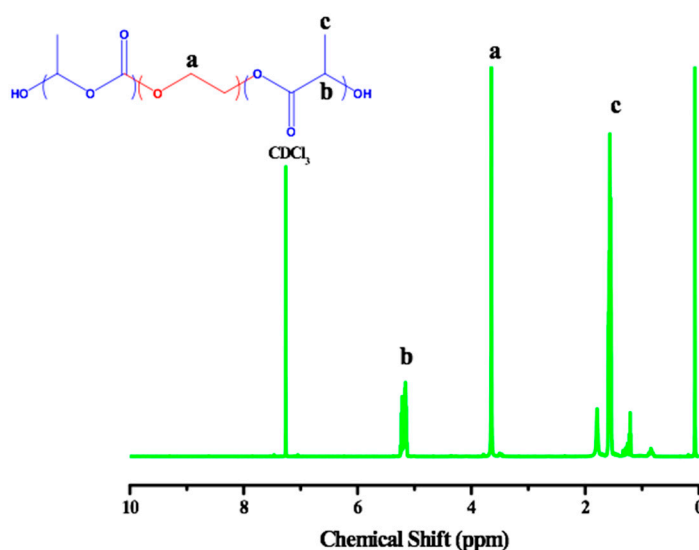


Figure 1. ¹H NMR spectrum of LEL triblock copolymer.

We used FTIR spectra to investigate the hydrogen bonding interaction in phenolic/LEL blends, as shown in Figure 2. The PLA block segment exhibited a free C=O group at 1756 cm⁻¹, as shown in Figure 2a, and no shoulder peak corresponding to hydrogen-bonded C=O was observed. However, only the free C=O group was gradually shifted to a lower wavenumber with the increase of phenolic concentration and was located at 1752 cm⁻¹ for the phenolic/LEL = 70/30 blend, indicating a weak hydrogen bonding interaction in the phenolic/PLA binary domain. In our previous studies, we determined that the inter-association equilibrium constant (K_A) for phenolic/PLA blend was smaller than 10, which is quite different to phenolic blends with other carbonyl-based polymers such as PVAc ($K_A = 83$) [58], PCL ($K_A = 116$) [55], or PAS ($K_A = 64$) [59]. Figure 2b displays the C–O–C absorption in phenolic/LEL blends. The PEO segment exhibited C–O–C absorption at 1090 cm⁻¹, and this peak shifted to 1088 cm⁻¹, which also corresponded to the hydrogen bonding interaction of the phenolic/PEO binary domain. Since ether absorption is highly conformationally sensitive, it was hard to calculate the K_A value; however, we calculated the K_A value for phenolic/PEO blend ($K_A = 264$) indirectly by using phenolic/PEO/PCL ternary blend [55]. Based on this result, we determined that the OH unit of the phenolic generally preferred to interact with PEO rather than PLA in the phenolic/LEL blends.

Figure 3a presents the SAXS patterns of various phenolic/LEL blends recorded at room temperature. It clearly displays the scattering patterns with the peak ratios of 1:√3 for phenolic/LEL = 70/30, 60/40, and 50/50 blends, corresponding to cylindrical structures. In addition, the first peaks at $q^* = 0.127 \text{ nm}^{-1}$ ($d = 49.4 \text{ nm}$), 0.074 nm^{-1} ($d = 84.8 \text{ nm}$), and 0.105 nm^{-1} ($d = 59.8 \text{ nm}$) for phenolic/LEL = 70/30, 60/40, and 50/50 blends, respectively, suggest that the phenolic/LEL = 60/40 blend possessed the largest

d-spacing of all these blend systems. When the phenolic/LEL ratio was further decreased to 40/60, it displayed no peak, indicating a disordered structure at this composition.

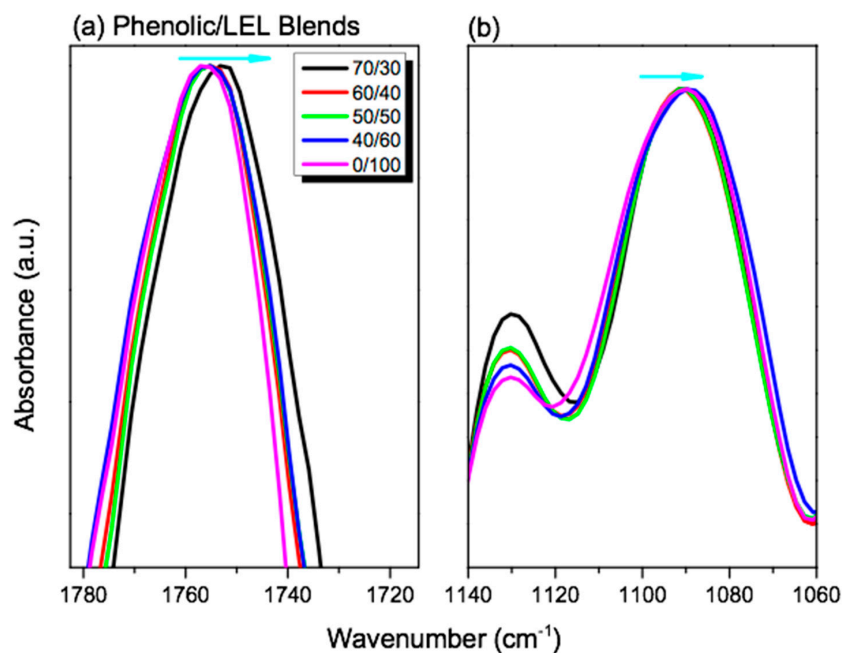


Figure 2. (a) C=O and (b) C–O–C absorptions of various phenolic/LEL blends based on FTIR spectra recorded at room temperature.

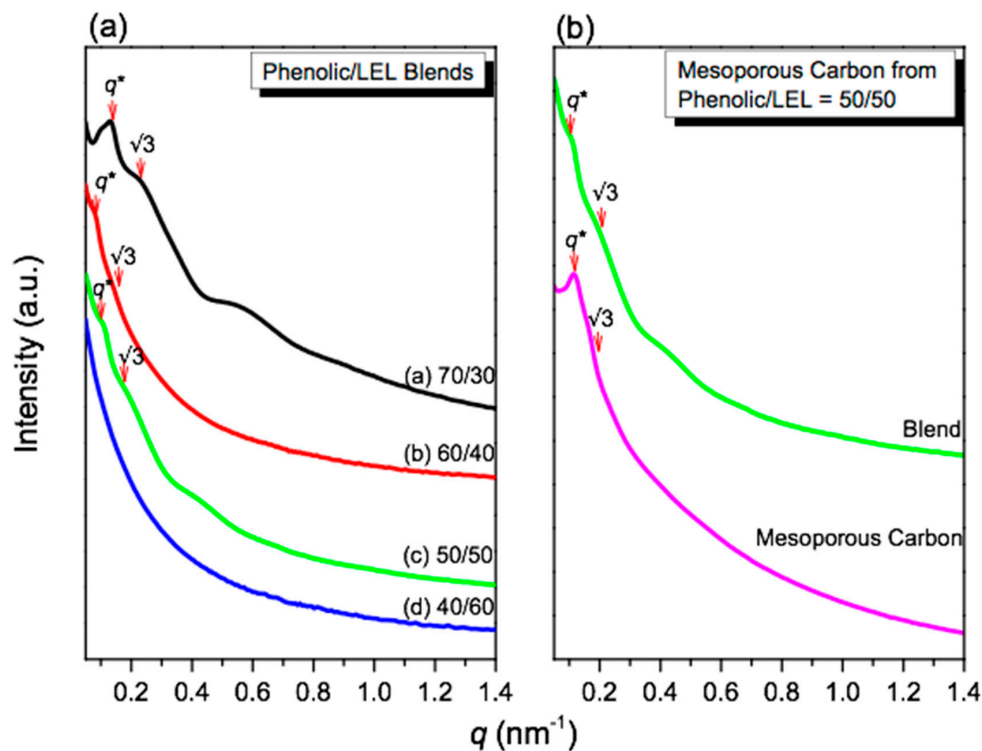


Figure 3. (a) SAXS patterns of various phenolic/LEL blends and (b) SAXS patterns of mesoporous carbon from phenolic/LEL = 50/50 blend.

3.2. Analyses of Mesoporous Carbons from Phenolic/LEL Blends

The mesoporous carbon could be obtained by thermal curing at 150 °C for 1 day using phenolic resin and LEL triblock copolymer as the template, which was removed by thermal calcination at 700 °C. Figure 3b compares the SAXS patterns of mesoporous carbon and its corresponding phenolic/LEL = 50/50 blend. We could observe that the peak ratio was maintained at 1:√3, but the first peak was shifted from $q^* = 0.105 \text{ nm}^{-1}$ ($d = 59.8 \text{ nm}$) to $q^* = 0.114 \text{ nm}^{-1}$ ($d = 55.1 \text{ nm}$) and became sharp after thermal calcination. This result indicates that the electron density contrast was increased and oxygen or hydrogen was removed to decrease the d -spacing by pore formation.

Figure 4 presents the SAXS pattern and TEM images of mesoporous carbons from the corresponding phenolic/LEL blends. Figure 4a displays the SAXS pattern of the mesoporous carbon from phenolic/LEL = 70/30 blend, in which there were two peaks found at low q value, suggesting two different pore sizes from the spherical or cylindrical structures. Peak ratios of 1:√3:√4:√7 were observed for the second q^* value, corresponding to the cylindrical structure. This was confirmed by the TEM image shown in Figure 4d and the corresponding pore size distribution based on the TEM image exhibited in Figure 4g with $26.5 \pm 4.9 \text{ nm}$. The SAXS patterns of the mesoporous carbon from phenolic/LEL = 60/40 and 50/50 blends presented in Figure 4b,c both displayed the peak ratios of 1:√3:√4, indicating the cylindrical structure, as observed by TEM images in Figure 4e,f. The pore size distributions based on TEM images were summarized and are displayed in Figure 4h ($54.0 \pm 11.6 \text{ nm}$) and Figure 4i ($36.8 \pm 9.2 \text{ nm}$). The mesoporous carbon with macroporous sizes (>50 nm), indicated the generation of macroporous/mesoporous carbon from the phenolic/LEL = 60/40 blend. Compared with the largest mesoporous carbon from the phenolic/PEO₁₁₄-*b*-PLA₉₄ = 60/40 blend with 21.0 nm in our previous work [50], the significantly increased pore size to 54.0 nm from the higher molecular weight of the template from phenolic/PLA₄₄₀-*b*-PEO₄₅₄-*b*-PLA₄₄₀ = 60/40 blend was expected.

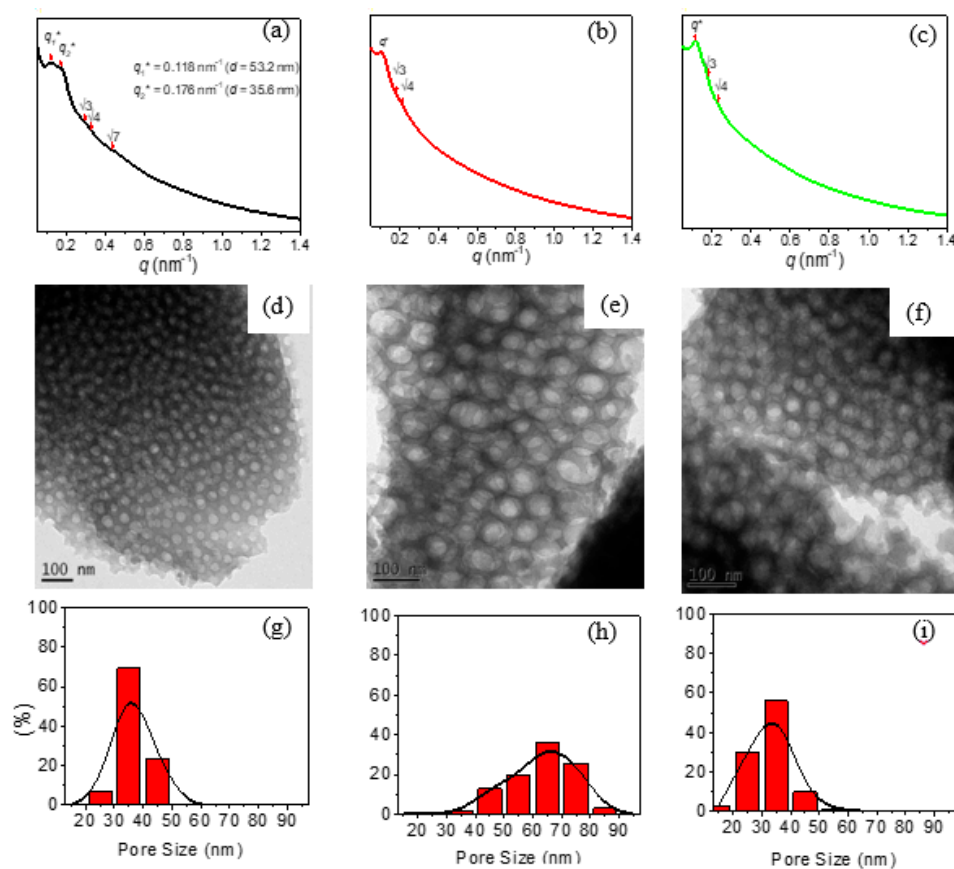


Figure 4. SAXS pattern, TEM image, and the corresponding pore size distribution of mesoporous carbons from phenolic/LEL blends of (a,d,g) 70/30, (b,e,h) 60/40, and (c,f,i) 50/50, respectively.

Nitrogen sorption isotherms were used to understand the corresponding pore structures of these mesoporous carbons as displayed in Figure 5a, in which typical IV curves all exhibited H₁-like hysteresis loops. The relative pressure (P/P_0) range from 0.85 to 1.0 was observed for the sharp capillary condensation steps, indicating porous structures with large and cylindrical pores. The results were consistent with the TEM images and SAXS patterns. The corresponding average mesoporous size distribution of these mesoporous carbons based on the Harkins and Jura model were 30.1 ± 11.3 , 45.6 ± 11.3 , and 44.7 ± 11.4 nm, as displayed in Figure 5b for phenolic/LEL = 70/30, 60/40, and 50/50 blends, respectively. Table 1 summarizes the pore sizes of the mesoporous carbons using BET and TEM analyses, d -spacing from SAXS analyses, surface area, and pore volume.

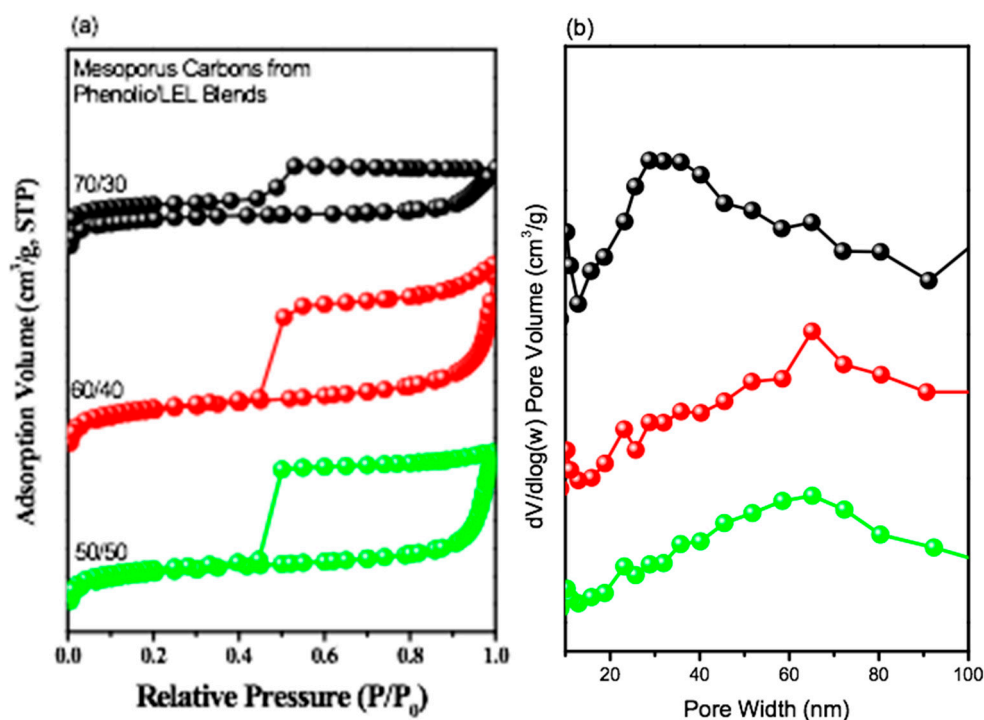


Figure 5. (a) N₂ adsorption isotherms and (b) pore size distributions of mesoporous carbons templated by various concentrations of LEL triblock copolymer.

Table 1. Physical properties of ultra-large mesoporous carbons templated by phenolic/PLA-*b*-PEO-*b*-PLA blends.

Phenolic/LEL	d Spacing (X-ray, nm)	Pore Size (BET, nm)	Pore Size (TEM, nm)	S_{BET} (m ² /g)	V_{Total} (cm ³ /g)	V_{Meso} (cm ³ /g)
70/30	51.2	30.1 ± 11.3	26.5 ± 4.9	441.3	0.27	0.18
60/40	61.6	45.6 ± 11.3	54 ± 11.6	609.7	0.48	0.23
50/50	54.9	44.7 ± 11.4	36.8 ± 9.2	564.2	0.42	0.19

3.3. Raman Spectra, CO₂ Capture Ability, and Electrochemical Analyses of Mesoporous Carbons

Raman spectra were used to understand the intrinsic behavior of the mesoporous carbons, as displayed in Figure 6. In general, the $I_{\text{D}}/I_{\text{G}}$ intensity ratios could be used to roughly indicate the degree of graphitization, where the intensity of D and G bands was due to the sp³ and sp² hybridized orbital of the C-C bond at 1320 and 1594 cm⁻¹, respectively [60–63]. The $I_{\text{D}}/I_{\text{G}}$ ratios for the mesoporous carbons from phenolic/LEL = 70/30, 60/40, and 50/50 blends were 2.58, 2.80, and 1.80, respectively, indicating the highly defected structure of mesoporous carbon from phenolic/LEL = 60/40 blend compared with the other mesoporous carbons.

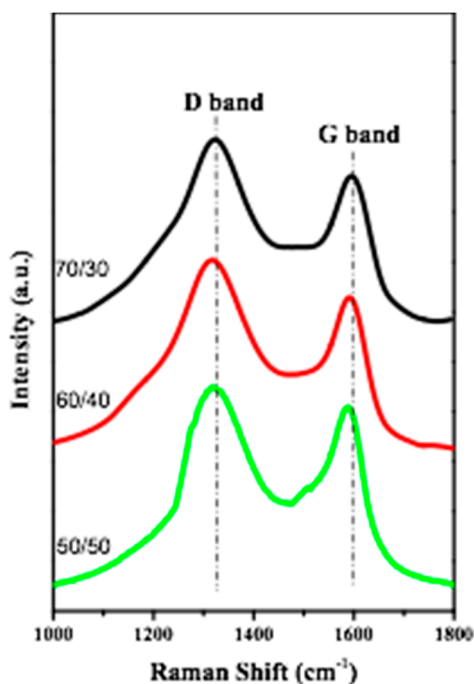


Figure 6. Raman spectra of mesoporous carbons templated by various concentrations of LEL triblock copolymer.

To explore the properties of the high surface area of these mesoporous carbons, we recorded the CO₂ adsorption isotherms for the mesoporous carbons at 25 and 0 °C, as presented in Figure 7, which exhibited the highest CO₂ capture ability of 4.05, 5.22, and 3.11 mmol/g at 298 K (Figure 7a) and 4.52, 6.19, and 4.13 mmol/g at 273 K (Figure 7b), respectively. Clearly, the mesoporous carbon from phenolic/LEL = 60/40 blend displayed the highest CO₂ capture of 5.22 and 6.19 mmol/g at 298 K and 273 K as compared with other mesoporous carbons at the same temperature due to possessing the highest specific surface area and defected structures. This result was also higher than other mesoporous carbons templated by other block copolymers or different materials [6,47,54,61,64,65].

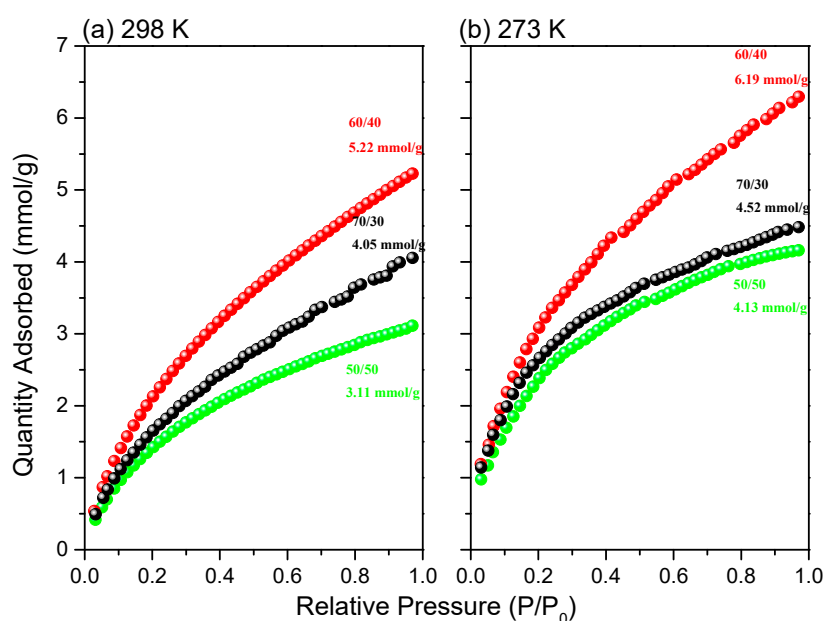


Figure 7. CO₂ capture behavior properties of mesoporous carbons templated by various concentrations of LEL triblock copolymer at (a) 298 K and (b) 273 K.

Using these mesoporous carbons in energy storage applications is essential to demonstrate their importance. Therefore, we selected mesoporous carbons from the phenolic/LEL = 60/40 blend to determine their electrochemical performance in a three-electrode cell using 1.0 M KCl as a green medium [66]. Figure 8a displays the CV curves for this mesoporous carbon with a wide potential window range from -1.0 to 1.0 V. The CV curves of the mesoporous carbon were representative of a wide electric double layer capacitor (EDLC) with minor pseudocapacitor (PC) properties. It showed a much higher area of EDLC at all scan rates, as observed in Figure 8b, and the capacitance value at $5\text{ mV}\cdot\text{s}^{-1}$ reached 120 F/g . This enhancement of the EDLC performance clearly reflects the major effect of the carbonization technique in providing a higher surface area for electron transfer on the electrode surface. The charge/discharge curves were tested at 2.0 A/g at the potential range (-1.0 to 1.0 V), as displayed in Figure 8c. The electrodes displayed efficient stability at 2.0 A/g for cycles, with 92% retentions and about 100% coulombic efficiency (Figure 8d). The charge/discharge curves showed typical symmetrical charge/discharge curves at the investigated current densities. Compared to other N-doped carbons and activated carbons, these results offered exceptional negligible IR drop curves with an excellent symmetric triangular shape and the longest potential range [67,68]. Besides, other porous carbons could not show such strong performance. In other words, these results were higher than those of other phenolic carbons used for energy storage, such as lignin-derived porous carbons, which reached a specific capacitance of 100 Fg^{-1} at 5 mV . These results are competitive with the results of other research with similar components [69,70]. The performance of an activated carton box with a surface area over $2700\text{ m}^2\text{ g}^{-1}$ has been investigated, and the obtained capacitance values exhibited a significant decline in retention and cycling abilities [71]. Our results are also much higher compared to other activated bamboo-like carbons composited with metal oxides [72]. Other comparable materials are summarized in Table S1 [73–78]. Therefore, we consider this mesoporous carbon to be a promising candidate for energy storage applications.

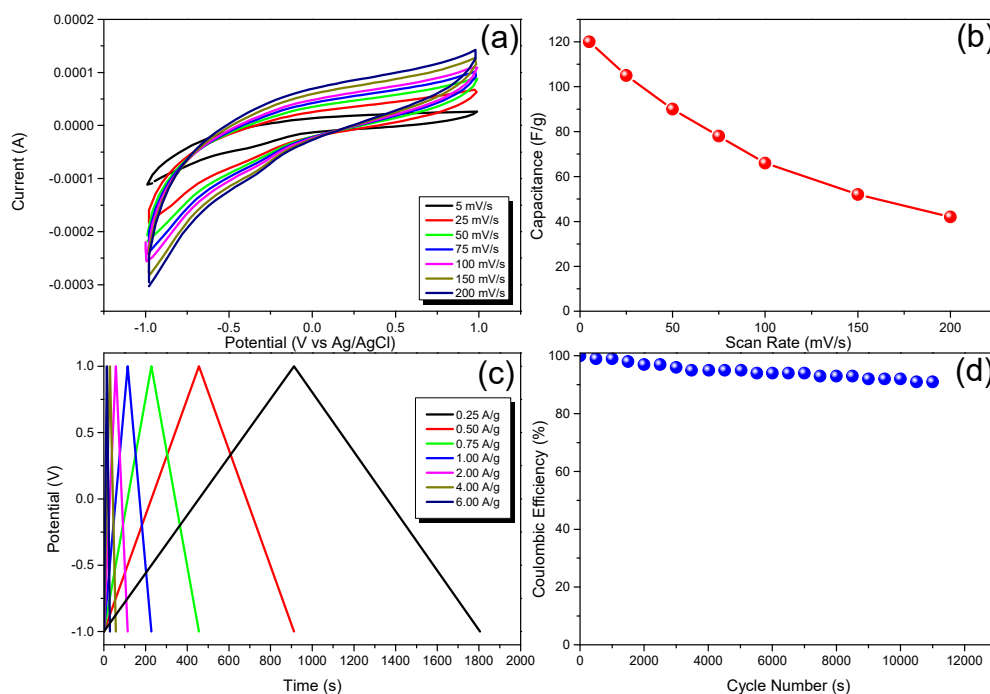


Figure 8. Mesoporous carbon from phenolic/LEL blend (60/40): (a) CV curves recorded at various scan rates; (b) capacitance plotted versus scan rate; (c) charge/discharge curves recorded at various current ranges; (d) coulombic efficiency recorded at 2.0 A/g for cycles.

4. Conclusions

Ultra-large mesoporous carbon (>50 nm) with high surface area (>600 m²/g) was successfully prepared using resol as the carbon source and templated using a high-molecular-weight LEL triblock copolymer as a single template. The self-assembled cylindrical structure of mesoporous carbons could be mediated by the hydrogen bonding interaction in the phenolic/PEO and phenolic/PLA phases after the thermal curing and carbonization procedures. The larger defected structure of mesoporous carbon from higher I_D/I_G value based on Raman spectra possessed higher CO₂ capture ability (6.19 mmol/g at 273 K), efficient capacitance properties (120 F/g at 5 mV s⁻¹), and excellent stability of 92% after many cycles. This study provides a facile method for the synthesis of large mesoporous carbon templated by LEL triblock copolymer for electrochemical and CO₂ capture applications.

Supplementary Materials: The following are available online at <http://www.mdpi.com/2073-4360/12/5/1193/s1>, Table S1: Comparison of different carbons with surface area and capacitance results.

Author Contributions: M.G.M., W.-S.H., and A.F.M.E.-M. conducted the experiment; M.M.M.A. completed the CV results; L.D. and T.C. helped to design the ROP and resol resin; S.-W.K. contributed to the literature review and the writing of this paper. All authors have read and agreed to the published version of the manuscript.

Funding: This research was funded by the Ministry of Science and Technology, Taiwan, under contracts MOST 106-2221-E-110-067-MY3 and MOST 105-2221-E-110-092-MY3, and also supported by the National Natural Science Foundation of China (Grants U and 51773214).

Conflicts of Interest: The authors declare no conflicts of interest.

References

1. Liu, J.; Xie, L.; Deng, J.; Gong, Y.; Tang, G.; Bai, H.; Wang, Y. Annular Mesoporous Carbonaceous Nanospheres from Biomass-Derived Building Units with Enhanced Biological Interactions. *Chem. Mater.* **2019**, *31*, 7186–7191. [[CrossRef](#)]
2. Chu, W.C.; Kim, J.; Kim, M.; Alshehri, A.A.; Alghamidi, Y.G.; Alzahrani, K.A.; Yamauchi, Y.; Malgras, V.; Kuo, S.W. Photodegradation Activity of Poly (ethylene oxide-*b*- ϵ -caprolactone)-Templated Mesoporous TiO₂ Coated with Au and Pt. *J. Nanosci. Nanotechnol.* **2020**, *20*, 5276–5281. [[CrossRef](#)] [[PubMed](#)]
3. Guo, Q.Y.; Zhang, B.X.; Feng, X.; Yan, X.Y.; Su, Z.; Cheng, S.Z.D.; Yue, K. Controlling the Periodically Ordered Nanostructures in Ceramics: A Macromolecule-Guided Strategy. *Macromol. Rapid Commun.* **2020**, *41*, 1900534–1900548. [[CrossRef](#)] [[PubMed](#)]
4. Jiang, B.; Guo, Y.; Kim, J.; Whitten, A.E.; Wood, K.; Kani, K.; Rowan, A.E.; Henzie, J.; Yamauchi, Y. Mesoporous Metallic Iridium Nanosheets. *J. Am. Chem. Soc.* **2018**, *140*, 12434–12441. [[CrossRef](#)]
5. Wang, J.; Xu, Y.; Ding, B.; Chang, Z.; Zhang, X.; Yamauchi, Y.; Wu, K.C.W. Confined Self-Assembly in Two-Dimensional Interlayer Space: Monolayered Mesoporous Carbon Nanosheets with In-Plane Orderly Arranged Mesopores and a Highly Graphitized Framework. *Angew. Chem. Int. Ed.* **2018**, *57*, 2894–2898. [[CrossRef](#)]
6. EL-Mahdy, A.F.M.; Young, C.; Kim, J.; You, J.; Yamauchi, Y.; Kuo, S.W. Hollow Microspherical and Microtubular [3 + 3] Carbazole-Based Covalent Organic Frameworks and Their Gas and Energy Storage Applications. *ACS Appl. Mater. Interface* **2019**, *11*, 9343–9354. [[CrossRef](#)]
7. Wang, C.; Wang, T.M.; Wang, Q.H. Ultralow-dielectric, nanoporous poly (methyl silsesquioxanes) films templated by a self-assembled block copolymer upon solvent annealing. *J. Polym. Res.* **2019**, *26*, 5. [[CrossRef](#)]
8. Wang, Z.B.; Qiang, H.W.; Zhang, C.L.; Zhu, Z.H.; Chen, M.; Chen, C.N.; Zhang, D.W. Facile fabrication of hollow polyaniline spheres and its application in supercapacitor. *J. Polym. Res.* **2018**, *25*, 129. [[CrossRef](#)]
9. El-Mahdy, A.F.M.; Mohamed, M.G.; Mansoure, T.H.; Yu, H.H.; Chen, T.; Kuo, S.W. Ultrastable tetraphenyl-*p*-phenylenediamine-based covalent organic frameworks as platforms for high-performance electrochemical supercapacitors. *Chem. Commun.* **2019**, *55*, 14890–14893. [[CrossRef](#)]
10. Wu, Y.C.; Lu, Y.S.; Bastakoti, B.P.; Li, Y.; Pramanik, M.; Hossain, M.S.; Yanmaz, E.; Kuo, S.W. Mesoporous TiO₂ Thin Film Formed from a Bioinspired Supramolecular Assembly. *ChemistrySelect* **2016**, *1*, 4295–4299. [[CrossRef](#)]

11. Tsai, C.C.; Gan, Z.; Kuo, S.W. Using benzoxazine chemistry and bio-based triblock copolymer to prepare functional porous polypeptide capable of efficient dye adsorption. *Polym. Chem.* **2018**, *9*, 3684–3693. [[CrossRef](#)]
12. Lu, Y.S.; Bastakoti, B.P.; Pramanik, M.; Malgras, V.; Yamauchi, Y.; Kuo, S.W. Direct Assembly of Mesoporous Silica Functionalized with Polypeptides for Efficient Dye Adsorption. *Chem. Eur. J.* **2016**, *22*, 1159–1164. [[CrossRef](#)] [[PubMed](#)]
13. Chu, W.C.; Peng, D.R.; Baskakoti, B.P.; Pramanik, M.; Malgras, V.; Ahamad, T.; Alshehri, S.M.; Yamauchi, Y.; Kuo, S.W. Co-templating Synthesis of Bimodal Mesoporous Silica for Potential Drug Carrier. *ChemistrySelect* **2016**, *1*, 1339–1346. [[CrossRef](#)]
14. Rouquerol, J.; Avnir, D.; Fairbridge, C.W.; Everett, D.H.; Haynes, J.M.; Pernicone, N.; Ramsay, J.D.F.; Sing, K.S.W.; Unger, K.K. Recommendations for the characterization of porous solids. *Pure Appl. Chem.* **1994**, *66*, 1739–1758. [[CrossRef](#)]
15. Langley, P.J.; Hulliger, J. Nanoporous and mesoporous organic structures: New openings for materials research. *Chem. Soc. Rev.* **1999**, *28*, 279–291. [[CrossRef](#)]
16. Dawson, R.; Cooper, I.; Adams, D.J. Nanoporous organic polymer networks. *Prog. Polym. Sci.* **2012**, *37*, 530–563. [[CrossRef](#)]
17. Muylaert, I.; Verberckmoes, A.; Decker, J.D.; Voort, P.V.D. Ordered mesoporous phenolic resins: Highly versatile and ultrastable support materials. *Adv. Colloid Interface Sci.* **2012**, *175*, 39–51. [[CrossRef](#)]
18. Li, J.G.; Chen, W.C.; Kuo, S.W. Phase behavior of mesoporous silicas templated by the amphiphilic diblock copolymer poly (ethylene-*b*-ethylene oxide). *Microporous Mesoporous Mater.* **2012**, *163*, 34–41. [[CrossRef](#)]
19. Kuo, S.W. *Hydrogen Bonding in Polymeric Materials*; John Wiley & Sons: Hoboken, NJ, USA, 2018.
20. Su, W.C.; Tsai, F.C.; Huang, C.F.; Dai, L.; Kuo, S.W. Flexible Epoxy Resins Formed by Blending with the Diblock Copolymer PEO-*b*-PCL and Using a Hydrogen-Bonding Benzoxazine as the Curing Agent. *Polymers* **2019**, *11*, 201. [[CrossRef](#)]
21. Dobrosielska, K.; Wakao, S.; Takano, A.; Matsushita, Y. Nanophase-separated structures of AB block copolymer/C homopolymer blends with complementary hydrogen-bonding interactions. *Macromolecules* **2008**, *41*, 7695–7698. [[CrossRef](#)]
22. Kwak, J.; Han, S.H.; Moon, H.C.; Kim, J.K.; Koo, J.; Lee, J.S.; Pryamitsyn, V.; Ganesan, V. Phase behavior of binary blend consisting of asymmetric polystyrene-block-poly (2-vinylpyridine) copolymer and asymmetric deuterated polystyrene-block-poly (4-hydroxystyrene) copolymer. *Macromolecules* **2015**, *48*, 1262–1266. [[CrossRef](#)]
23. Miyase, H.; Asai, Y.; Takano, A.; Matsushita, Y. Kaleidoscopic Tiling Patterns with Large Unit Cells from ABC Star-Shaped Terpolymer/Diblock Copolymer Blends with Hydrogen Bonding Interaction. *Macromolecules* **2017**, *50*, 979–986. [[CrossRef](#)]
24. Tsou, C.T.; Kuo, S.W. Competing Hydrogen Bonding Interaction Creates Hierarchically Ordered Self-Assembled Structures of PMMA-*b*-P4VP/PVPh-*b*-PS Mixtures. *Macromolecules* **2019**, *52*, 8374–8383. [[CrossRef](#)]
25. Mao, B.H.; EL-Mahdy, A.F.M.; Kuo, S.W. Bio-inspired multiple complementary hydrogen bonds enhance the miscibility of conjugated polymers blended with polystyrene derivatives. *J. Polym. Res.* **2019**, *26*, 208. [[CrossRef](#)]
26. Kwak, J.; Han, S.H.; Moon, H.C.; Kim, J.K. Effect of the degree of hydrogen bonding on asymmetric lamellar microdomains in binary block copolymer blends. *Macromolecules* **2015**, *48*, 6347–6352. [[CrossRef](#)]
27. Tseng, T.C.; Kuo, S.W. Hydrogen bonding induces unusual self-assembled structures from mixtures of two miscible disordered diblock copolymers. *Eur. Polym. J.* **2019**, *116*, 361–369. [[CrossRef](#)]
28. Tseng, T.C.; Kuo, S.W. Hierarchical Self-Assembled Structures from Diblock Copolymer Mixtures by Competitive Hydrogen Bonding Strength. *Molecules* **2018**, *23*, 2242. [[CrossRef](#)]
29. Tseng, T.C.; Kuo, S.W. Hydrogen-Bonding Strength Influences Hierarchical Self-Assembled Structures in Unusual Miscible/Immiscible Diblock Copolymer Blends. *Macromolecules* **2018**, *51*, 6451–6459. [[CrossRef](#)]
30. Su, W.C.; Wu, Y.S.; Wang, C.F.; Kuo, S.W. Self-Assembled Structures of Diblock Copolymer/Homopolymer Blends through Multiple Complementary Hydrogen Bonds. *Crystals* **2018**, *8*, 330. [[CrossRef](#)]
31. Soler-Illia, G.J.; Crepaldi, E.L.; Grosso, D.; Sanchez, C. Block copolymer-templated mesoporous oxides. *Curr. Opin. Colloid Interface Sci.* **2003**, *8*, 109–126. [[CrossRef](#)]

32. Wei, J.; Wang, H.; Deng, Y.; Sun, Z.; Shi, L.; Tu, B.; Luqman, M.; Zhao, D. Solvent evaporation induced aggregating assembly approach to three-dimensional ordered mesoporous silica with ultralarge accessible mesopores. *J. Am. Chem. Soc.* **2011**, *133*, 20369–20377. [[CrossRef](#)] [[PubMed](#)]
33. Li, J.G.; Lin, Y.D.; Kuo, S.W. From Microphase Separation to Self-Organized Mesoporous Phenolic Resin through Competitive Hydrogen Bonding with Double-Crystalline Diblock Copolymers of Poly (ethylene oxide-*b*- ϵ -caprolactone). *Macromolecules* **2011**, *44*, 9295–9309. [[CrossRef](#)]
34. Li, J.G.; Chu, W.C.; Jeng, U.; Kuo, S.W. In Situ Monitoring of the Reaction-Induced Self-Assembly of Phenolic Resin Templated by Diblock Copolymers. *Macromol. Chem. Phys.* **2013**, *214*, 2115–2123. [[CrossRef](#)]
35. Liu, C.C.; Chu, W.C.; Li, J.G.; Kuo, S.W. Mediated Competitive Hydrogen Bonding Form Mesoporous Phenolic Resins Templated by Poly (ethylene oxide-*b*- ϵ -caprolactone-*b*-l-lactide) Triblock Copolymers. *Macromolecules* **2014**, *47*, 6389–6400. [[CrossRef](#)]
36. Zhao, D.; Feng, J.; Huo, Q.; Melosh, N.; Fredrickson, G.H.; Chmelka, B.F.; Stucky, G.D. Triblock copolymer syntheses of mesoporous silica with periodic 50 to 300 angstrom pores. *Science* **1998**, *279*, 548–552. [[CrossRef](#)] [[PubMed](#)]
37. Chu, W.C.; Chiang, S.F.; Li, J.G.; Kuo, S.W. Mesoporous silicas templated by symmetrical multiblock copolymers through evaporation-induced self-assembly. *RSC Adv.* **2014**, *4*, 784–793. [[CrossRef](#)]
38. Kosonen, H.; Ruokolainen, J.; Torkkeli, M.; Serimaa, R.; Nyholm, P.; Ikkala, O. Micro- and macrophase separation in phenolic resol resin/PEO-PPO-PEO block copolymer blends: Effect of hydrogen-bonded PEO length. *Macromol. Chem. Phys.* **2002**, *203*, 388–392. [[CrossRef](#)]
39. Liang, C.; Dai, S. Synthesis of mesoporous carbon materials via enhanced hydrogen-bonding interaction. *J. Am. Chem. Soc.* **2016**, *128*, 5316–5317. [[CrossRef](#)]
40. Meng, Y.; Gu, D.; Zhang, F.; Shi, Y.; Cheng, L.; Feng, D.; Wu, Z.; Chen, Z.; Wan, Y.; Stein, A.; et al. A family of highly ordered mesoporous polymer resin and carbon structures from organic-organic self-assembly. *Chem. Mater.* **2006**, *18*, 4447–4464. [[CrossRef](#)]
41. Chu, W.C.; Chiang, S.F.; Li, J.G.; Kuo, S.W. Hydrogen bonding-mediated microphase separation during the formation of mesoporous novolac-type phenolic resin templated by the triblock copolymer, PEO-*b*-PPO-*b*-PEO. *Materials* **2013**, *6*, 5077–5093. [[CrossRef](#)]
42. Deng, Y.; Yu, T.; Wang, Y.; Shi, Y.; Meng, Y.; Gu, D.; Zhang, L.; Huang, Y.; Liu, C.; Wu, X.; et al. Ordered mesoporous silicas and carbons with large accessible pores templated from amphiphilic diblock copolymer poly (ethylene oxide)-*b*-polystyrene. *J. Am. Chem. Soc.* **2007**, *29*, 1690–1697. [[CrossRef](#)] [[PubMed](#)]
43. Bloch, E.; Llewellyn, P.L.; Phan, T.; Bertin, D.; Hornebecq, V. On defining a simple empirical relationship to predict the pore size of mesoporous silicas prepared from PEO-*b*-PS diblock copolymers. *Chem. Mater.* **2009**, *21*, 48–55. [[CrossRef](#)]
44. Hu, D.; Xu, Z.; Zeng, K.; Zheng, S. From self-organized Novolac resins to ordered nanoporous carbons. *Macromolecules* **2010**, *43*, 2960–2969. [[CrossRef](#)]
45. Chu, W.C.; Bastakoti, B.P.; Kaneti, Y.V.; Li, J.G.; Alamri, H.R.; Allothman, Z.A.; Yamauchi, Y.; Kuo, S.W. Tailored Design of Bicontinuous Gyroid Mesoporous Carbon and Nitrogen-Doped Carbon from Poly (ethylene oxide-*b*-caprolactone) Diblock Copolymers. *Chem. Eur. J.* **2017**, *23*, 13734–13741. [[CrossRef](#)] [[PubMed](#)]
46. Li, J.G.; Ho, Y.F.; Ahmed, M.M.M.; Liang, H.C.; Kuo, S.W. Mesoporous Carbons Templated by PEO-PCL Block Copolymers as Electrode Materials for Supercapacitors. *Chem. Eur. J.* **2019**, *25*, 10456–10463. [[CrossRef](#)]
47. EL-Mahdy, A.F.M.; Liu, T.E.; Kuo, S.W. Direct Synthesis of Nitrogen-Doped Mesoporous Carbons from Triazine-Functionalized Resol for CO₂ Uptake and Highly Efficient Removal of Dyes. *J. Hazard. Mater.* **2020**, *391*, 122163. [[CrossRef](#)] [[PubMed](#)]
48. Deng, Y.; Liu, C.; Gu, D.; Yu, T.; Tu, B.; Zhao, D. Thick wall mesoporous carbons with a large pore structure templated from a weakly hydrophobic PEO-PMMA diblock copolymer. *J. Mater. Chem.* **2008**, *18*, 91–97. [[CrossRef](#)]
49. Altukhov, O.; Kuo, S.W. Crystallization ability of poly (lactic acid) block segments in templating poly (ethylene oxide-*b*-lactic acid) diblock copolymers affects the resulting structures of mesoporous silicas. *RSC Adv.* **2015**, *5*, 22625–22637. [[CrossRef](#)]
50. Li, J.G.; Lee, P.Y.; Ahmed, M.M.M.; Mohamed, M.G.; Kuo, S.W. Varying the Hydrogen Bonding Strength in Phenolic/PEO-*b*-PLA Blends Provides Mesoporous Carbons Having Large Accessible Pores Suitable for Energy Storage. *Macromol. Chem. Phys.* **2020**, *221*, 2000040. [[CrossRef](#)]

51. Werner, J.G.; Hoheisel, T.N.; Wiesner, U. Synthesis and characterization of gyroidal mesoporous carbons and carbon monoliths with tunable ultralarge pore size. *ACS Nano* **2014**, *8*, 731–743. [[CrossRef](#)]
52. Deng, Y.; Liu, J.; Liu, C.; Gu, D.; Sun, Z.; Wei, J.; Zhang, J.; Tu, B.; Zhao, D. Ultra-large-pore mesoporous carbons templated from poly (ethylene oxide)-b-polystyrene diblock copolymer by adding polystyrene homopolymer as a pore expander. *Chem. Mater.* **2008**, *20*, 7281–7286. [[CrossRef](#)]
53. Wei, J.; Deng, Y.; Zhang, J.; Sun, Z.; Tu, B.; Zhao, D. Large-pore ordered mesoporous carbons with tunable structures and pore sizes. *Solid State Sci.* **2011**, *13*, 784–792. [[CrossRef](#)]
54. Hung, W.S.; Ahmed, M.M.M.; Mohamed, M.G.; Kuo, S.W. Competing Hydrogen Bonding Produces Mesoporous/Macroporous Carbons Templated by a High-Molecular-Weight Poly (caprolactone–b–ethylene oxide–b–caprolactone) Triblock Copolymer. *J. Polym. Res.* **2020**, *27*, 173. [[CrossRef](#)]
55. Kuo, S.W.; Lin, C.L.; Chang, F.C. Phase Behavior and Hydrogen Bonding in Ternary Polymer Blends of Phenolic Resin/Poly (ethylene oxide)/Poly (ϵ -caprolactone). *Macromolecules* **2002**, *35*, 278–285. [[CrossRef](#)]
56. Huang, C.F.; Kuo, S.W.; Lin, F.J.; Huang, W.J.; Wang, C.F.; Chen, W.Y.; Chang, F.C. Influence of PMMA-Chain-End Tethered Polyhedral Oligomeric Silsesquioxanes on the Miscibility and Specific Interaction with Phenolic Blends. *Macromolecules* **2006**, *39*, 300–308. [[CrossRef](#)]
57. Huang, C.F.; Kuo, S.W.; Lin, H.C.; Chen, J.K.; Chen, Y.K.; Xu, H.; Chang, F.C. Thermal properties, miscibility and specific interactions in comparison of linear and star poly (methyl methacrylate) blend with phenolic. *Polymer* **2004**, *45*, 5913–5921. [[CrossRef](#)]
58. Huang, M.W.; Kuo, S.W.; Wu, H.D.; Chang, F.C.; Fang, S.Y. Miscibility and hydrogen bonding in blends of poly (vinyl acetate) with phenolic resin. *Polymer* **2002**, *43*, 2479–2487. [[CrossRef](#)]
59. Kuo, S.W.; Chang, F.C. Miscibility Behavior and Specific Interaction of Phenolic Resin with Poly (acetoxystyrene) Blends. *Macromol. Chem. Phys.* **2002**, *203*, 868–878. [[CrossRef](#)]
60. Mukherjee, S.; Das, M.; Manna, A.; Krishna, R.; Das, S. Dual Strategic Approach to Prepare Defluorinated Triazole-Embedded Covalent Triazine Frameworks with High Gas Uptake Performance. *Chem. Mater.* **2019**, *31*, 3929–3940. [[CrossRef](#)]
61. Mohamed, M.G.; EL-Mahdy, A.F.M.; Ahmed, M.M.M.; Kuo, S.W. Direct Synthesis of Microporous Bicarbazole-Based Covalent Triazine Frameworks for High-Performance Energy Storage and Carbon Dioxide Uptake. *ChemPlusChem* **2019**, *84*, 1767–1774. [[CrossRef](#)]
62. Hao, L.; Ning, J.; Luo, B.; Wang, B.; Zhang, Y.; Tang, Z.; Yang, J.; Thomas, A.; Zhi, L. Structural Evolution of 2D Microporous Covalent Triazine-Based Framework toward the Study of High-Performance Supercapacitors. *J. Am. Chem. Soc.* **2015**, *137*, 219–225. [[CrossRef](#)] [[PubMed](#)]
63. Wang, Y.; Dong, L.; Lai, G.; Wei, M.; Jiang, X.; Bai, L. Nitrogen-Doped Hierarchically Porous Carbons Derived from Polybenzoxazine for Enhanced Supercapacitor Performance. *Nanomaterials* **2019**, *9*, 131. [[CrossRef](#)] [[PubMed](#)]
64. Mohamed, M.G.; EL-Mahdy, A.F.M.; Takashi, Y.; Kuo, S.W. Ultrastable conductive microporous covalent triazine frameworks based on pyrene moieties provide high-performance CO₂ uptake and supercapacitance. *New J. Chem.* **2020**. [[CrossRef](#)]
65. Abuzeid, H.R.; EL-Mahdy, A.F.M.; Kuo, S.W. Hydrogen Bonding Induces Dual Porous Types with Microporous and Mesoporous Covalent Organic Frameworks Based on Bicarbazole Units. *Microporous Mesoporous Mater.* **2020**, *300*, 110151. [[CrossRef](#)]
66. Yu, L.; Hu, L.; Anasori, B.; Liu, Y.T.; Zhu, Q.; Zhang, P.; Gogotsi, Y.; Xu, B. MXene-Bonded Activated Carbon as a Flexible Electrode for High-Performance Supercapacitors. *ACS Energy Lett.* **2018**, *3*, 1597–1603. [[CrossRef](#)]
67. Abioye, A.M.; Ani, F.N. Recent Development in the Production of Activated Carbon Electrodes from Agricultural Waste Biomass for Supercapacitors: A Review. *Renew. Sustain. Energy Rev.* **2015**, *52*, 1282–1293. [[CrossRef](#)]
68. Farzana, R.; Rajarao, R.; Bhat, B.R.; Sahajwalla, V. Performance of an Activated Carbon Supercapacitor Electrode Synthesised from Waste Compact Discs (CDs). *J. Ind. Eng. Chem.* **2018**, *65*, 387–396. [[CrossRef](#)]
69. Wang, D.; Fang, G.; Xue, T.; Ma, J.; Geng, G. A Melt Route for the Synthesis of Activated Carbon Derived from Carton Box for High Performance Symmetric Supercapacitor Applications. *J. Power Sources* **2016**, *307*, 401–409. [[CrossRef](#)]
70. Zhou, X.; Chen, Q.; Wang, A.; Xu, J.; Wu, S.; Shen, J. Bamboo-like Composites of V₂O₅/Polyindole and Activated Carbon Cloth as Electrodes for All-Solid-State Flexible Asymmetric Supercapacitors. *ACS Appl. Mater. Interfaces* **2016**, *8*, 3776–3783. [[CrossRef](#)]

71. Ahmed, M.M.M.; Imae, T.; Hill, J.P.; Yamauchi, Y.; Ariga, K.; Shrestha, L.K. Defect-Free Exfoliation of Graphene at Ultra-High Temperature. *Coll. Surf. A Physicochem. Eng. Asp.* **2018**, *538*, 127–132. [[CrossRef](#)]
72. Goldfarb, J.L.; Dou, G.; Salari, M.; Grinstaff, M.W. Biomass-Based Fuels and Activated Carbon Electrode Materials: An Integrated Approach to Green Energy Systems. *ACS Sustain. Chem. Eng.* **2017**, *5*, 3046–3054. [[CrossRef](#)]
73. Zhai, S.; Jiang, W.; Wei, L.; Karahan, H.E.; Yuan, Y.; Ng, A.K.; Chen, Y. All-carbon solid-state yarn supercapacitors from activated carbon and carbon fibers for smart textiles. *Mater. Horiz.* **2015**, *2*, 598–605. [[CrossRef](#)]
74. Cao, J.; Jafta, C.J.; Gong, J.; Ran, Q.; Lin, X.; Félix, R.; Wilks, R.G.; Bär, M.; Yuan, J.; Ballauff, M.; et al. Synthesis of Dispersible Mesoporous Nitrogen-Doped Hollow Carbon Nanoplates with Uniform Hexagonal Morphologies for Supercapacitors. *ACS Appl. Mater. Interfaces* **2016**, *8*, 29628–29636. [[CrossRef](#)] [[PubMed](#)]
75. Park, H.; Ambade, R.B.; Noh, S.H.; Eom, W.; Koh, K.H.; Ambade, S.B.; Lee, W.J.; Kim, S.H.; Han, T.H. Porous Graphene-Carbon Nanotube Scaffolds for Fiber Supercapacitors. *ACS Appl. Mater. Interfaces* **2019**, *11*, 9011–9022. [[CrossRef](#)] [[PubMed](#)]
76. Yang, C.M.; Kim, Y.J.; Miyawaki, J.; Kim, Y.A.; Yudasaka, M.; Iijima, S.; Kaneko, K. Effect of the Size and Position of Ion-Accessible Nanoholes on the Specific Capacitance of Single-Walled Carbon Nanohorns for Supercapacitor Applications. *J. Phys. Chem. C* **2015**, *119*, 2935–2940. [[CrossRef](#)]
77. Stimpfling, T.; Leroux, F. Supercapacitor-Type Behavior of Carbon Composite and Replica Obtained from Hybrid Layered Double Hydroxide Active Container. *Chem. Mater.* **2010**, *22*, 974–987. [[CrossRef](#)]
78. Thirukumaran, P.; Atchudan, R.; Parveen, A.S.; Lee, Y.R.; Kim, S.C. Polybenzoxazine originated N-doped mesoporous carbon ropes as an electrode material for high-performance supercapacitors. *J. Alloy. Compd.* **2018**, *750*, 384–391. [[CrossRef](#)]



© 2020 by the authors. Licensee MDPI, Basel, Switzerland. This article is an open access article distributed under the terms and conditions of the Creative Commons Attribution (CC BY) license (<http://creativecommons.org/licenses/by/4.0/>).

© 2020. This work is licensed under <http://creativecommons.org/licenses/by/3.0/> (the “License”). Notwithstanding the ProQuest Terms and Conditions, you may use this content in accordance with the terms of the License.